INVITED PAPER *Special Section on Electronic Displays*

Universal Angle Visibility Realized by a Volumetric 3D Display Using a Rotating Mirror-Image Helix Screen

Karin WAKATSUKI[†], ***Nonmember***, **Chiemi FUJIKAWA**[†a)], ***and*** **Makoto OMODANI**[††], ***Members***

SUMMARY Herein, we propose a volumetric 3D display in which cross-sectional images are projected onto a rotating helix screen. The method employed by this display can enable image observation from universal directions. A major challenge associated with this method is the presence of invisible regions that occur depending on the observation angle. This study aimed to fabricate a mirror-image helix screen with two helical surfaces coaxially arranged in a plane-symmetrical configuration. The visible region was actually measured to be larger than the visible region of the conventional helix screen. We confirmed that the improved visible region was almost independent of the observation angle and that the visible region was almost equally wide on both the left and right sides of the rotation axis.

key words: *3D, visible region, volumetric display, helix screen*

1. Introduction

Binocular stereo displays are currently the most popular 3D system; however, they have certain limitations. For example, they only offer a single of viewpoint [1]–[4] or limited number of viewpoints [5], [6], and users often need to wear special eyeglasses [7]. They cannot provide a side nor backside view of objects. Conversely, volumetric 3D displays, which provide light pixels in a real 3D space, can enable observation from universal directions without the need for special eyeglasses [8]–[16]. Typical volumetric displays have been developed using rotating light emitting diode (LED) arrays; however, they suffer from not only mechanical difficulty due to rotating heavy LED arrays but also low resolution [17]–[21].

We have been focusing on another type of volumetric display method by which multilayers of cross-sectional images are formed on a rotating helix screen by a projector synchronized with the rotation speed [22]–[28]. This 3D system, however, has one potential problem: the blind region is partially assumed in the cylindrical display volume formed by the rotating helix screen [29], [30]. In this study, a novel shape helix screen was developed to expand the visible region, and the enlarged visible region was actually measured.

Manuscript received March 9, 2023.
Manuscript revised May 31, 2023.
Manuscript publicized August 3, 2023.
[†]The authors are with Tokai University, Hiratsuka-shi, 259–1292 Japan.
[††]The author is with Tokyo Denki University, Hikigun, 350–0394 Japan.
a) E-mail: chiemi@tokai.ac.jp
DOI: 10.1587/transele.2023DII0003

2. 3D Display System Using a Helix Rotating Screen and the Causes of Residual Invisible Regions

An arrangement of our 3D display system is shown in Fig. 1. This 3D display system consists of a digital mirror device (DMD) projector (Table 1) and an opaque helix screen (Fig. 2; height of the helix surface: 83.6 mm, radius: 41.8 mm). The opaque helix screen was fabricated using a 3D printer (Table 2). The cross-sectional images were projected synchronized with the trigger pulses from the high-speed rotating helix screen. The cross-sectional images of 128 layers were projected for each rotation in our prototype. The DMD projector projected multilayers of cross-sectional images onto the rotating helix screen. Three-dimensional images were formed by the accumulated afterimages of the projected cross-sectional images. The rotation speed of the screen was set to 1800 rpm, which afforded smooth afterimages without flickering.

Figure 3 shows an example of the displayed 3D images. The 3D images of a skull could be observed from all directions. However, some part of the 3D image appears to be missing depending on the observation angle θ (Fig. 1). Figure 3 (c) is a displayed image observed from the horizontal

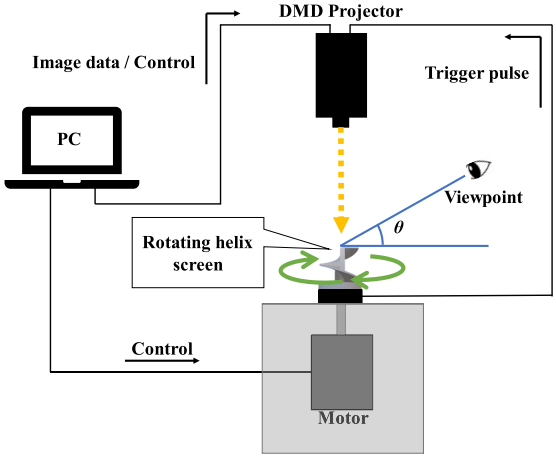

Fig. 1 Arrangement of the proposed 3D display system.

Table 1 Specifications of the projector used.

Item	Specification
Device	ViALUX GmbH: STAR-07 RGB
Throw ratio	1.8
Brightness	1100 lm

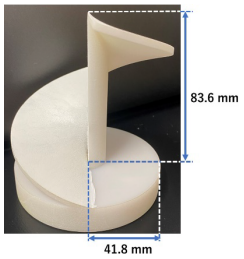

Fig. 2 Opaque helix screen.

Table 2 Specifications of the 3D printers for screen fabrication.

Item	For fabricating an opaque helix screen	For fabricating a transparent helix screen
Device	3D systems, Inc.: ProJet® MJP 5500X	D-MEC Ltd.: ACCULAS® BA-85S
Method	MultiJet Printing	Stereolithography Technology
Resin	VisiJet CR-WT 200	SCR786
Layer resolution	16 µm	100 µm

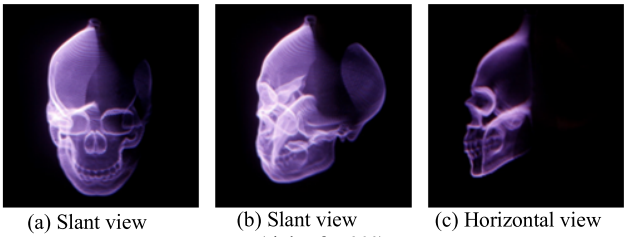

(a) Slant view (front, $\theta = 30°$) (b) Slant view (right, $\theta = 30°$) (c) Horizontal view ($\theta = 0°$)

Fig. 3 Typical 3D images (opaque helix screen).

direction of the screen. The right side of the 3D image is not visible. Two factors can cause the occurrence of invisible regions. The first is that the main body of the helix screen sometimes blocks the light path from the helix surface to the viewpoint. The second is that the screen surface is sometimes viewed from behind when the viewpoint is low. The 3D image is not visible when viewed from behind the projection surface. The second cause can be solved using a transparent helix screen [31]. However, the first issue cannot be solved by simply using a transparent helix screen. The displayed image cannot be clearly observed through the transparent screen because the obstructive transparent screen surface is generally not perpendicular to the light path from the displayed image to the eyes of an observer. The transparent helix screen fabricated using a 3D printer (Table 2) is shown in Fig. 4 (a). The displayed image on a transparent helix screen is shown in Fig. 5 (a). The visibility of the displayed image significantly decreased when the transparent helix screen was used, attributed to the decrease in the amount of scattered light from the screen. As a solution, the helix surface of the screen was coated with a scattering material to increase the amount of scattered light from the screen. Figure 4 (b) shows a semi-transparent helix screen coated with talc powder on its surface. Figure 5 (b) shows the displayed image on the semi-transparent helix screen. The displayed image of the left half in Fig. 5 (b) is still darker

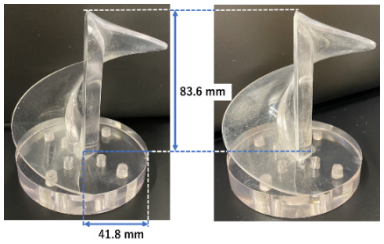

(a) Transparent type (b) Semi-transparent type

Fig. 4 Two types of helix screens.

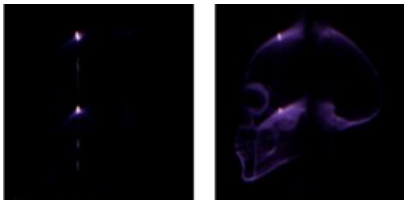

(a) Transparent type (b) Semi-transparent type

Fig. 5 Three-dimensional images displayed by each type of helix screen.

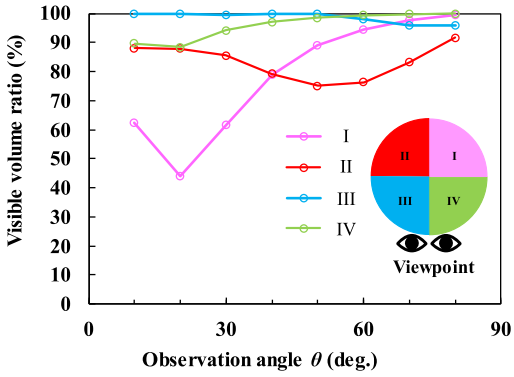

Fig. 6 Calculated visible volume ratio of the transparent type of screen in the four quadrants (simulation results).

than that of in Fig. 3 (c). However, the displayed image of the right half in Fig. 5 (b) is brighter and clearer than that of in Fig. 3 (c). A comparison of the displayed images in Fig. 5 (b) and Fig. 3 (c) indicates that the visible region is larger on the semi-transparent helix screen. Figure 6 shows the visible volume ratio (= [visible volume]/[cylindrical whole volume formed by rotating helix screen]) of the transparent and semi-transparent helix screens calculated by a simulation using the ray tracing method. The simulation was calculated assuming that the displayed image is not visible through the screen. Figure 6 shows the dependence of the visible volume ratio on the observation angle θ. The displaying volume formed by the rotating helix screen was divided into quadrants in Cartesian coordinates. Figure 6 shows that invisible regions remain even when a transparent (or semi-transparent) helix screen is used. The cause of the residual invisible region is assumed to be the blocking of the light path from the helical surface to the viewpoint by the main body of the helix screen.

3. Proposal of a Mirror-Image Helix Screen

A mirror-image helix screen (Fig. 7) is proposed herein. The mirror-image helix screen comprises a pair of helixes with a clockwise downslope and clockwise upslope facing each other plane symmetrically. The mirror-image helix screen is expected to have the following four advantages.
(1) The visible region is expected to be enlarged. Two helical surfaces scan all displaying volumes once during one screen rotation. The cross-sectional images have two chances of projection to the twin helical surfaces. Two light spots are always projected at the same position in the displaying volume. Figure 8 shows how the two helixes function compensatively. The part of the yellow helix circled in red in Fig. 8 (a) is blocked by the blue helix and is not visible to the observer in front of the helix screen. The same position in the display volume is in the visible condition in the following scan, as shown in Fig. 8 (b).
(2) The invisible regions due to lack of brightness are reduce. Figure 9 (a) shows the helix surface observed from a direction parallel to the surface. The displayed image is not visible due to a lack of diffuse light in the direction of the eyes. Figure 9 (b) shows the other helix surface observed from the same viewpoint as in Fig. 9 (a). The observation angle is almost perpendicular to the surface, and the displayed image is visible because of sufficient diffuse light reaching the eye.
(3) The difference in brightness of the displayed image in each area decreases. The semi-transparent helix screen typically does not possess the same transmittance and reflectance; consequently, the brightnesses of the transmitted and reflected lights are different. The light point in a mirror-image helix screen is observed in the afterimage composite of the transmitted and reflected lights. Thus, the brightness difference of each image pixel decreases.
(4) The brightness of the displayed image when the mirror-image helix screen is used is twice that when a single helix screen is used. This is because the helix pair always provides two chances of projection to every position in the display volume.

The mirror-image helix screen composed of transparent material was fabricated using a 3D printer. The displayed image of the mirror-image helix screen is expected to possess a wider visible region and uniform image brightness. Figure 10 (a) shows a photograph of the screen. The 3D printer used to fabricate the mirror-image helix screen is the same as that used to fabricate the transparent helix screen (Table 2). The mirror-image helix screen was also coated

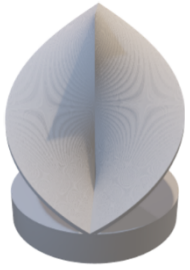

Fig. 7 Proposed shape of the mirror-image helix screen.

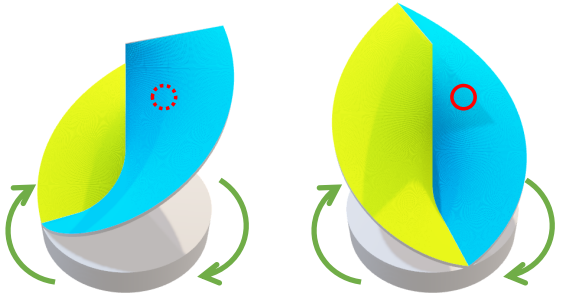

(a) Region I on the yellow slope is invisible (b) Region I on the blue slope is visible

Fig. 8 Complementary display functions of the two slopes.

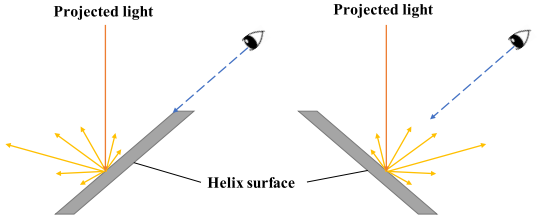

(a) Viewing from a position parallel to the screen (b) Viewing from a position perpendicular to the screen

Fig. 9 Differences in the diffuse light arrival at the same viewpoint.

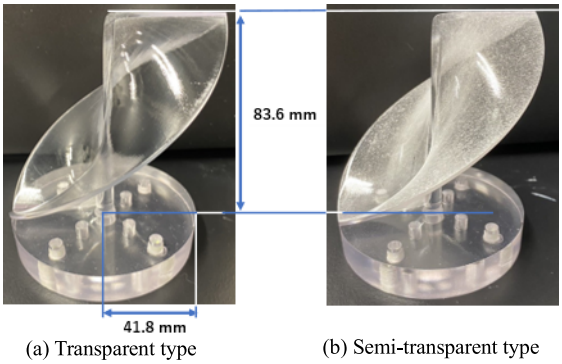

(a) Transparent type (b) Semi-transparent type

Fig. 10 Two types of mirror-image helix screens.

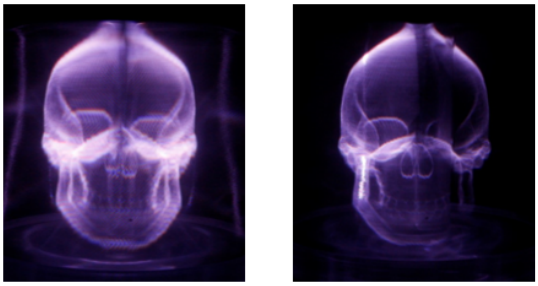

(a) Mirror-image helix screen (b) Helix screen

Fig. 11 Three-dimensional images displayed by each type of screen.

with white talc powder (Fig. 10 (b)) to increase the amount of scattered light. Figure 11 (a) shows the 3D image of the skull displayed on the mirror-image helix screen. When the mirror-image helix screen was used, the image visibility improved, especially on the right side of the skull, compared to that of the displayed image (Fig. 11 (b)) when the conventional helix screen was used. Moreover, the 3D image by the mirror-image helix screen showed superior uniformity in image brightness.

4. Measurement of the Visible Region Formed by the Mirror-Image Helix Screen

The visible regions of the mirror-image helix screen and helix screen were measured and compared. The visible volume ratio was calculated by simulation at the observation angle θ = 10°–80°. The visible volume ratio of the simulation does not consider the amount of light reaching the eyes as a result of reflection and transmission on the screen in the actual projection environment. This implies that a display region may be judged as a visible region even when the amount of light from the region is not sufficient to offer a visible image.

Thus, we actually measured displaying volumes by counting number of visible image segments formed by the mirror-image helix screen and by the helix screen. Image segments (a cube with sides of 2 mm) were displayed in 880 representative positions in the displaying volume formed by the rotating screen. The 880 image segments were placed with a spacing of 8 mm between each other (Fig. 12). The distance from the camera to the screen was set to 500 mm, the same distance as that of the setting condition in the simulation, to compare the measured results of the visible volume ratio with the simulation results by the ray tracing method. The image segments were captured by a camera placed with the observation angle θ shown in Fig. 13. The photographs of the image segments were binarized to black and white. The maximum brightness of the non-projected area was used as the binarization threshold. The number of white image segments after binarization was counted as the number of visible image segments. The ratio of the number of visible image segments to the number of projected image segments was calculated as the percentage of the visible volume ratio for each display area divided into each quadrant (Fig. 6). The measurements were performed in the θ range of 0°–50°, because the observation angle θ is limited to < 50° in our prototype system due to positional interference to the viewpoints by the projector and its base panel (Fig. 13).

Figure 14 shows the results of the visibility evaluation of the image segments offered by the semi-transparent helix screen (Fig. 4 (b)). The measured result shows a lower visible volume ratio than does the simulation result, suggesting that the visible regions in the simulation included regions that were not visible due to a lack of brightness.

Figure 15 shows the results of the visibility evaluation of the image segments displayed on the mirror-image helix screen. The visible volume ratio of the mirror-image helix screen exceeds 80% at observation angles θ from 0° to 50°, indicating that the visible volume ratio is almost independent of the observation angle θ in this range. Remarkably, the curves of the visible volume ratio are almost identical between regions I and II and between regions III and IV. The regional difference in the visible volume ratio of the helix screen was eliminated using the mirror-image helix screen.

Increase rates of the visible volume ratio offered by the mirror-image helix screen were calculated and compared with those of the visible volume ratio of the helix screen. The superiority ratio the mirror-image helix screen R is given by

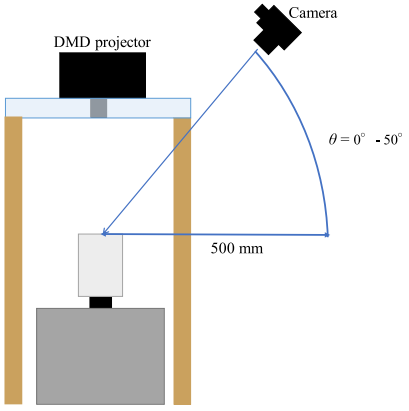

Fig. 13 Measurement conditions for capturing the image segments.

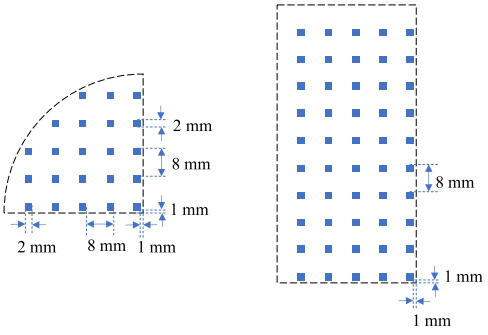

(a) Top view (b) Side view

Fig. 12 Arrangement of the 3D image segments.

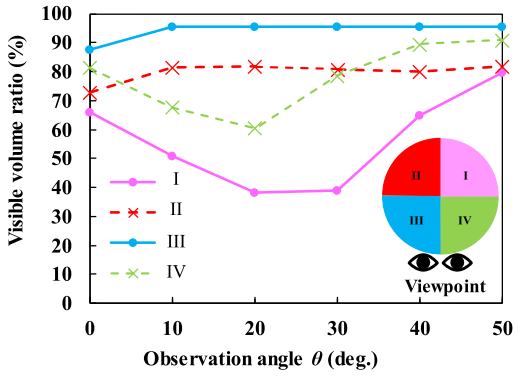

Fig. 14 Measured visible volume ratio of the helix screen.

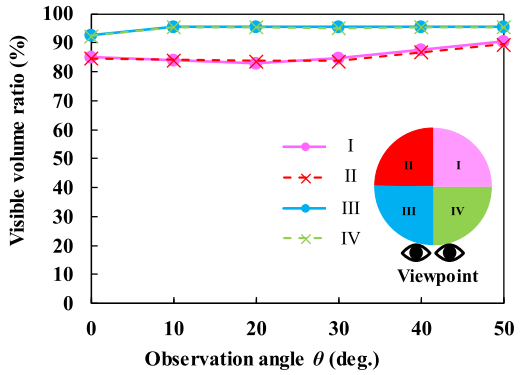

Fig. 15 Measured visible volume ratio of the mirror-image helix screen.

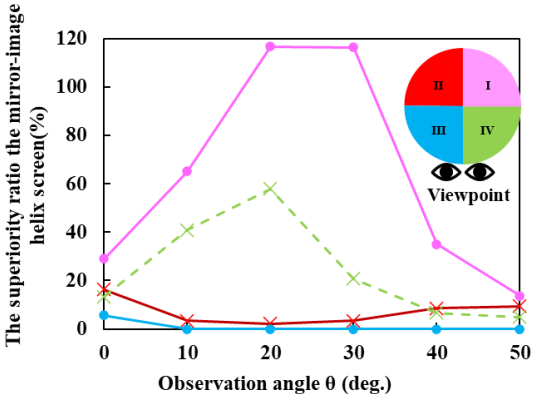

Fig. 16 Comparison between the visible volume ratios by the mirror-image helix screen and helix screen.

$$R = (V_2 - V_1)/V_1, \tag{1}$$

where V_1 is the visible volume ratio of the helix screen, and V_2 is the visible volume ratio of the mirror-image helix screen. Calculated results by Eq. (1) are shown in Fig. 16. The mirror-image helix screen shows a remarkable increase of the superiority ratio, in Fig. 16, in the right regions I and IV, especially at the observation angle θ = 10°–30°.

5. Conclusion

We have developed a novel mirror-image helix screen in order to expand the visible region of our volumetric 3D displays, and we have actually measured the enlargement of the visible region. The followings are the summarized results of our study.

1) A novel mirror-image helix screen was developed to enlarge the visible regions, which is a significant challenge for 3D display systems that use helix screens.
2) The invisible regions of the mirror-image helix screen were smaller than those of the helix screen, primarily in the right region at viewing angles of 10°–30°.
3) We confirmed that the visible volume ratio offered by the mirror-image helix screen always exceeds 80% at observation angles of 0°–50° and that the visible volume ratio is almost independent of the observation angle.
4) The measured visible volume ratio of the mirror-image helix screen was almost equal between the left and right sides of the rotation axis; hence, the pending problem of left–right difference in the visibility of the 3D image was eliminated.

References

[1] J. Geng, "Three-dimensional display technologies," Adv Opt. Photonics, vol.5, no.4, pp.456–535, 2013.
[2] E.A. Edirisinghe and J. Jiang, "Stereo Imaging, an Emerging Technology," presented at the SIGGRA, L'Aquila, 2000.
[3] S.E.B. Sorensen, P.S. Hansen, and N.L. Sorensen, U.S. Patent, no.6687003, 2004.
[4] T. Iwasaki, T. Kubota, and A. Tawara, "The tolerance range of binocular disparity on a 3D display based on the physiological characteristics of ocular accommodation," Displays, vol.30, no.1, pp.44–48, 2009.
[5] D. Brewaster, "The stereoscope; its history, theory, and construction, with its application to the fine and useful arts and to education," John Murray, London, 1856.
[6] K. Perlin, S. Paxia, and J.S. Kollin, Proc. ACM SIGGRAPH, pp.319–324, 2000.
[7] G.D. Love, D.M. Hoffman, P.J.W. Hands, J. Gao, A.K. Kirby, and M.S. Banks, "High-speed switchable lens enables the development of a volumetric stereoscopic display," Opt. Express, vol.17, no.18, pp.15716–15725, 2009.
[8] B.G. Blundell and A.J. schwarz, Volumetric three-dimensional display systems, Wiley-IEEE Press, New York, 2000.
[9] O.S. Cossairt, J. Napoli, S.L. Hill, R.K. Dorval, and G.E. Favalora, "Occlusion-capable multiview volumetric three-dimensional Display," Appl. Opt., vol.46, no.8, pp.1244–1250, 2007.
[10] E. Downing, R. Hesselink, J. Ralston, and R. Macfarlane, "A Three-Color, Solid-State, Three-Dimensional Display," Science, vol.273, no.5279, pp.1185–1189, 1996.
[11] M. Halle, "Autostereoscopic displays and computer graphics," ACM SIGGRAPH Computer Graphics, vol.31, no.2, pp.58–62, 1997.
[12] Z.J. Geng, U.S. Patent, no.6064423, 2000.
[13] J. Geng, "Volumetric 3D Display for Radiation Therapy Planning," J. Disp. Technol., vol.4, no.4, pp.437–450, 2008.
[14] H.H. Refai, "Static Volumetric Three-Dimensional Display," J. Disp. Technol., vol.5, no.10, pp.391–397, 2009.
[15] D. Miyazaki, T. Honda, K. Ohno, and T. Mukai, "Volumetric Display System Using a Digital Micromirror Device Based on Inclined-Plane Scanning," J. Disp. Technol., vol.6, no.10 pp.548–552, 2010.
[16] Barry G. Blundell, About 3D Volumetric Displays, Publisher Walker & Wood Limited, New Zealand, 2011.
[17] G. Favalora, D.M. Hall, M. Giovinco, J. Napoli, and R.K. Dorval, "A Multi-Megavoxel Volumetric 3-D Display System for Distributed Collaboration," Proc. IEEE GlobeCom 2000 Workshop, 2001.
[18] J. Wu, X. Liu, C. Yan, X.X. Xia, and H. Li, "The analysis of colour uniformity for a volumetric display based on a rotating LED array," J. Opt., vol.13, no.5, 055501, 2011.
[19] R.J. Schipper, U.S. Patent, no.3097261, 1963.
[20] E.P. Berlin, U.S. Patent, no.4160973, 1979.
[21] M. Gately, Y. Zhai, M. Yeary, E. Petrich, and L. Sawalha, "A Three-Dimensional Swept Volume Display Based on LED Arrays," Journal of Display Technology, vol.7, no.9, pp.503–514, 2011.
[22] F. Tain, H. Wang, Y. Fang, H. Pan, and X. Xia, "A Swept Volume Display System Using a Planetary Gear Structure Based on Parallel Moving," J. Disp. Technol., vol.8, no.8, 457–463, 2012.
[23] J. Geng, "A volumetric 3D display based on a DLP projection engine," Displays, vol.34, no.1, pp.39–48, 2013.
[24] J. Geng, U.S. Patent, no.0062684, 2005.
[25] R.K. Dorval, M. Thomas, and J.L. Bareau, U.S. Patent, no.6554430,

2003.
[26] C. Yan, X. Liu, H. Li, X. Xia, H. Lu, and W. Zheng, "Color three-dimensional display with omnidirectional view based on a light-emitting diode projector," Appl. Opt., vol.48, no.22, pp.4490–4495, 2009.
[27] M. Hirsch, U.S. Patent, no.2967905, 1961.
[28] G.E. Favalora, "Volumetric 3D Displays and Application Infrastructure," Computer, vol.38, no.8, pp.37–44, 2005.
[29] K. Wakatsuki, C. Fujikawa, and M. Omodani, "Volumetric 3D Display using a Rotating Spiral Screen - Evaluation of the Visible Region -," Proc. International Display Workshop 28, 3Dp1-9L, pp.501–504, 2021.
[30] K. Wakatsuki, C. Fujikawa, and M. Omodani, "Evaluation of visible region in volumetric 3D display using a rotating helix screen," Jpn. J. Appl. Phys., vol.61, no.6, 062055, 2022.
[31] K. Wakatsuki, C. Fujikawa, and M. Omodani, "Dependence of 3D Image Contrast on Ceiling/Background Illumination and Screen Reflectance in a Volumetric Display using a Helix Rotating Screen," Proc. International Display Workshop 29, 3D5-4L, pp.567–570, 2022.

Karin Wakatsuki received her B.S. in engineering from Tokai University in 2021. She is expected to receive her M.S. degree from Tokai University in 2023. She is now engaged in the research of the volumetric 3D displays at the graduate school of Tokai University.

Chiemi Fujikawa received her Ph.D. from Toyota Technological Institute in 1999. She joined Department of Optical and Imaging Science and Technology, in the School of Engineering, of Tokai University in 2006 as a lecturer. Her current position is a professor of Department of Information Media Technology, in the School of Information Science and Technology, of Tokai University. She is now engaged in optical functional devices, 3D display technologies, and free space optical communication.

Makoto Omodani received his B.S. and M.S. in mechanical engineering from Tohoku University in 1978 and 1980, respectively, and his Ph.D. from Tokyo University in 1987. He joined NTT in 1980 working on printing technologies at Yokosuka Electrical Communication Laboratories. He moved to Tokai University in 1997. He has moved to Tokyo Denki University in 2020. His current position is a professor of Division of Information Systems and Design, in the School of Science and Engineering of Tokyo Denki University. He is now engaged in digital imaging technologies including 3D and e-Paper technologies.